Intensity-Driven Adaptive-Neighborhood Technique for Polarimetric and Interferometric SAR Parameters Estimation

Gabriel Vasile, *Student Member, IEEE*, Emmanuel Trouvé, *Member, IEEE*, Jong-Sen Lee, *Life Fellow, IEEE*, and Vasile Buzuloiu, *Senior Member, IEEE*

***Abstract*—In this paper, a new method to filter coherency matrices of polarimetric or interferometric data is presented. For each pixel, an adaptive neighborhood (AN) is determined by a region growing technique driven exclusively by the intensity image information. All the available intensity images of the polarimetric and interferometric terms are fused in the region growing process to ensure the validity of the stationarity assumption. Afterward, all the pixels within the obtained AN are used to yield the filtered values of the polarimetric and interferometric coherency matrices, which can be derived either by direct complex multilooking or from the locally linear minimum mean-squared error (LLMMSE) estimator. The entropy/alpha/anisotropy decomposition is then applied to the estimated polarimetric coherency matrices, and coherence optimization is performed on the estimated polarimetric and interferometric coherency matrices. Using this decomposition, unsupervised classification for land applications by an iterative algorithm based on a complex Wishart density function is also applied. The method has been tested on airborne high-resolution polarimetric interferometric synthetic aperture radar (POL-InSAR) images (Oberpfaffenhofen area—German Space Agency). For comparison purposes, the two estimation techniques (complex multilooking and LLMMSE) were tested using three different spatial supports: a fix-sized symmetric neighborhood (boxcar filter), directional nonsymmetric windows, and the proposed AN. Subjective and objective performance analysis, including coherence edge detection, receiver operating characteristics plots, and bias reduction tables, recommends the proposed algorithm as an effective POL-InSAR postprocessing technique.**

***Index Terms*—Coherency estimation, interferometry, multivariate region growing, polarimetric synthetic aperture radar.**

I. Introduction

A SYNTHETIC aperture radar (SAR) system measures both amplitude and phase of the backscattered signal, producing one complex image for each recording. The principle of SAR interferometry (InSAR) relies on the acquisition of two such complex images under slightly different viewing angles. After the two initial images are coregistered, the normalized complex cross-correlation is computed. The most commonly known measures in interferometry are its magnitude, namely the *coherence*, and its *phase*. The coherence is usually used to describe the temporal and spatial variations of the acquired signal. The phase includes a geometrical component directly linked to the distance between the target and the sensor positions, providing the height information of the target.

In order to estimate the coherence, the required ensemble averages are replaced by spatial averages: a number of L neighboring pixels are averaged to yield an estimate of the coherence and phase image (operation called "complex multilooking"). However, despite this initial estimation, both coherence and phase images are highly corrupted by speckle. Hence, the need to improve coherence estimation arises in order to reduce the estimation bias and variance [1], [2]. The use of larger window sizes with fixed shapes gives unsatisfactory results, since the stationarity assumption is often no longer valid and the final resolution decreases.

Polarimetric synthetic aperture radar (POLSAR) is an extension of the SAR imaging system, the sensors being able to emit and receive two polarizations. Monostatic polarimetric acquisitions are characterized by the 3×3 polarimetric coherency matrix. The POLSAR information allows the discrimination of different scattering mechanisms. The first characteristic decomposition of the coherency matrix for target scattering decomposition was proposed in [3]. The received signal can be split into a sum of three scattering contributions with orthogonal polarimetric signatures. The orthonormal eigenvectors of the Hermitian target coherency matrix are used for analyzing the eigenvector space. The dominant scattering mechanism is represented by the largest eigenvalue of the coherency matrix. In [4] and [5], Cloude and Pottier introduced the target entropy and the $H - \alpha$ model by assigning to each eigenvector the corresponding coherent single scattering mechanism. Based on this decomposition, unsupervised classification for land applications was performed by an iterative algorithm based on complex Wishart density function [6], [7].

Interferometry in POLSAR performs two acquisitions (spatially separated by the baseline) of the scattering matrix for each resolution cell. The advantages of interferometry (height and/or displacement information) are enhanced by the polarimetric decomposition techniques. In [8], Cloude and Papathanassiou applied the polarimetric basis transformations in the POL-InSAR

Manuscript received June 28, 2005; revised November 10, 2005.

G. Vasile is with the Laboratoire d'Informatique, Systèmes, Traitement de l'Information et de la Connaissance, Université de Savoie-ESIA-BP, 806-74016 Annecy Cedex, France, and also with the Image Processing and Analysis Laboratory, "Politehnica" University of Bucharest, Bucharest 061071, Romania (e-mail: gabriel.vasile@univ-savoie.frl; gvasile@alpha.imag.pub.ro).

E. Trouvé is with the Laboratoire d'Informatique, Systèmes, Traitement de l'Information et de la Connaissance, Université de Savoie-ESIA-BP, 806-74016 Annecy Cedex, France (e-mail: emmanuel.trouve@univ-savoie.fr).

J.-S. Lee is with the Remote Sensing Division, Naval Research Laboratory, Washington, DC 20375-5351 USA (e-mail: jong.lee@nrl.navy.mil).

V. Buzuloiu is with the Image Processing and Analysis Laboratory, "Politehnica" University of Bucharest, Bucharest 061071, Romania (e-mail: buzuloiu@alpha.imag.pub.ro).

Digital Object Identifier 10.1109/TGRS.2005.864142

case and obtained interferograms between all possible linear combination of polarization states. As polarization and interferometric coherence are tightly related, an optimization algorithm based on the maximization of the interferometric coherence is proposed [8], [9].

A filtering step is very often required to finally obtain reliable estimates of the complex cross-correlation. Moreover, the high resolution of newly available SAR airborne images offers the opportunity to observe much thinner spatial features than the lower resolution of the up-to-now available SAR images. Being able to preserve such a high resolution in robust estimations of POL-InSAR coherency is an important issue to make this information useful.

Different speckle filtering strategies proposed over the last 20 years have been reviewed for one-channel SAR images in [10] and [11]. To handle the scene nonstationarity issue, two different models, namely the multiplicative speckle model and the product model, yield to two different filtering approaches. The first approach is based on the assumption of local stationarity and yields to different filters which search for local neighborhoods respecting this assumption and use adaptive estimators such as the local linear minimum mean square error (LLMMSE) [12], [13]. The second approach corresponds to nonstationary speckle models which require to introduce prior knowledge on the scene such as the distribution of the intensity mean in the gamma filter [14] or multilevel pdfs in multiply stochastic models [15], [16].

The review and the experimental results presented on intensity images in [11] encourage the use of the first approach with multiresolution techniques for optimal parameter estimation. Most techniques developed to extend estimation windows and respect signal local stationarity are based on tests and thresholds which allow windows to grow in different directions when spatial features are detected. The technique proposed by Wu and Maître [17] selects maximum homogeneous regions by testing the evolution of the standard deviation σ when the window size increases, after splitting in one of the eight possible directions if necessary. Three thresholds are empirically chosen to test four cases: point-target, close or on step edge, and homogeneous area. This filter has been improved by Nicolas *et al.* [18] with two modifications. First, the standard deviation σ is replaced by the equivalent number of look L which is linked to the coefficient of variation CV (normalized standard deviation) by $\sigma/\mu = 1/\sqrt{L}$ for intensity images. Secondly, the estimation of L is based on the low-order moments, second kind cumulant method which yields a low variance estimator with analytically known variance linked to the number of sample used in the estimation windows. This allows the authors to take the estimator variance into account when comparing L with the theoretical number of looks and analyzing the evolution of L between the current window and the increased size windows. A different strategy was proposed by Hagg and Sties [19] to test local stationarity on directional subwindows of decreasing size: starting from large window size such as 11×11, directional subwindows are tested and size is reduced by 2 until the local estimate of the CV is found to be lower than the corresponding global estimate of the coefficient of variation. These global estimates are obtained on the whole image for different window size by fitting χ^2 distributions with the beginning of the CV histograms. The multiresolution technique proposed in [11] combines these different techniques by including specific feature detectors (point targets, lines, edges) to test successively different kind of nonstationarity. The main characteristics of these techniques is the use of homogeneous/nonhomogeneous tests to select (sub)windows of larger size (pixels are not tested and aggregated individually). These "window tests" are based on CV local estimates and require to take into account the fact that CV estimated on small windows is lower than the theoretical CV.

In the framework of POL-InSAR imagery, a spatially adaptive filtering method for improving the accuracy of the coherency estimation was introduced in [20]. Eight directional subwindows are defined in order to locate the most homogeneous area inside the considered neighborhood. The subwindow selection procedure is driven by the average of the available span images of the interferometric pair. The pixels within the selected subwindow are used to yield the filtered covariance matrix, which is derived from the locally linear minimum mean-squared error (LLMMSE) estimator of the 6×6 covariance matrix

$$\widetilde{[C]}_6 = \overline{[C]}_6 + b([C]_6 - \overline{[C]}_6). \tag{1}$$

In (1), $\overline{[C]}_6$ stands for the average value of the POL-InSAR covariance matrix computed in the given subwindow, while $b \in [0, 1]$ is a locally computed weight that measures the local stationarity.

This paper presents a new spatially adaptive algorithm for coherency matrix estimation. Around each pixel, an adaptive neighborhood (AN) is formed using a region growing technique rather different from the previous "window growing" techniques: pixels are tested one by one and progressively aggregated if they belong to the same statistical population as the initial pixel. Moreover, the region growing algorithm is driven by all the available intensity images (the terms corresponding to the main diagonal of the roughly estimated coherency matrix). Pixels belonging to an adaptive "intensity-driven region" are more likely to respect the local stationarity hypothesis than pixels belonging to a squared fixed size window. Finally, the algorithm estimates the coherency matrix either by direct complex multilooking or from the LLMMSE estimator. The two estimation techniques were tested using three different spatial supports: a fix-sized symmetric neighborhood (boxcar filter), directional nonsymmetric windows, and the proposed AN. The effectiveness of this proposed method is demonstrated using L-band E-SAR polarimetric interferometric data.

The remainder of this paper is organized as follows. In Section II, the principles of polarimetric InSAR are reviewed in more detail. Section III is dedicated to the presentation of the proposed intensity-driven adaptive-neighborhood (IDAN) estimation and its application to LLMMSE filtering. In Section IV the results obtained using the proposed filter are presented and compared to those given by the boxcar and directional filtering methods. Results of entropy-alpha-anisotropy decomposition and coherence optimization, followed by a Wishart classification are also given. Eventually, in Section V, some conclusions and perspectives are presented.

II. Polarimetric SAR Images

The POL-InSAR data are obtained by two parallel passes separated by a baseline for interferometry. By using the Pauli basis marices [8], the obtained coherent scattering vectors $[k]_i$ are closer to the physical phenomena of wave scattering

$$[k]_i = \frac{1}{\sqrt{2}} \begin{bmatrix} S_{HH_i} + S_{VV_i} \\ S_{HH_i} - S_{VV_i} \\ 2S_{XX_i} \end{bmatrix}. \tag{2}$$

One complete representation of the data is the 6×6 Hermitian positive semidefinite coherency matrix

$$[T]_6 = E\left\{ \begin{bmatrix} [k]_1 \\ [k]_2 \end{bmatrix} \begin{bmatrix} [k]_1^{*T} & [k]_2^{*T} \end{bmatrix} \right\} = \begin{bmatrix} [T]_{11} & [\Omega]_{12} \\ [\Omega]_{12}^{*T} & [T]_{22} \end{bmatrix} \tag{3}$$

where $E\{\dots\}$ denotes the expectation value, $[T]_{ii}$ are the 3×3 polarimetric coherency positive semidefinite Hermitian matrices from each pass, $[\Omega]_{12}$ being the interferometric coherency matrix between the polarized acquisitions

$$[T]_{ii} = E\left\{ [k]_i [k]_i^{*T} \right\} \qquad [\Omega]_{12} = E\left\{ [k]_1 [k]_2^{*T} \right\}. \tag{4}$$

While the scatter vector, expressed either in lexicographic basis or in Pauli basis, is usually modeled by a multivariate complex Gaussian probability density function (pdf), the obtained coherency matrix $[T_6]$ defined in (3) follows a complex Wishart pdf [7], [21]. The diagonal elements of the coherency matrix have the same speckle statistics as conventional single channel SAR images.

A. H/α/A Decomposition

To extract useful information from POLSAR data, several polarimetric decompositions have been introduced: Huynen [22], Krogager [23], Cameron [24], Freeman-Durden [25], or TSVM [26]. In [5], Cloude and Pottier proposed a decomposition based on the projection of the coherency matrix $[T]$ onto its eigenvalues basis. The matrix $[T]$ is given by a weighted sum of three unitary matrices of rank one, each representing a pure scattering mechanism $[T^{(i)}]$

$$[T] = \sum_{i=1}^{3} \lambda_i [v]_i [v]_i^{*T} = \sum_{i=1}^{3} \lambda_i \left[T^{(i)} \right] \tag{5}$$

where $\lambda_1 > \lambda_2 > \lambda_3$ are the ordered eigenvalues and v_i its corresponding eigenvectors. The entropy H and anisotropy A have been defined as

$$H = \sum_{i=1}^{3} -P_i \log_3 P_i \tag{6}$$

$$A = \frac{\lambda_2 - \lambda_3}{\lambda_2 + \lambda_3} \tag{7}$$

where the pseudoprobabilities P_i are given by

$$P_i = \frac{\lambda_i}{\sum_{j=1}^{3} \lambda_j}. \tag{8}$$

Also, the α parameter is given as the weighted mean of the α_i parameters corresponding to the three scattering mechanisms [5]

$$\alpha = \sum_{i=1}^{3} P_i \alpha_i. \tag{9}$$

The extracted two meaningful roll-invariant parameters H and α indicate the random behavior of the global scattering and, respectively, the mean scattering mechanism from surface to double bounce scattering. They are strongly related to the geophysical properties of the ground target area providing reliable classification information. In [5], nine clustering zones are proposed in the H and α plane.

Being already implemented in POLSAR processing software as POLSARpro (European Space Agency) or RAdar Tools [27], the H/α/A decomposition has been chosen to illustrate the benefit of the proposed filtering methods.

B. Coherence Optimization

Due to the strong influence of the polarization upon the estimate of the interferometric coherence, Cloude and Papathanassiou proposed a method for finding the optimal linear combination of polarization states [8]. The optimum scattering mechanism corresponds to the projection of both master and slave target vectors on the eigenvectors $[w]_{1_{\text{opt}}}$ and $[w]_{2_{\text{opt}}}$ of the maximum eigenvalues. The highest coherence γ_{opt1} is obtained by forming the interferogram between the two optimized scalar complex images $\mu_{1\text{opt}}$ and $\mu_{2\text{opt}}$

$$\begin{aligned} \mu_{1\text{opt}} \mu_{2\text{opt}}^{*} &= \left([w]_{1\text{opt}}^{*T} [k]_1 \right) \left([w]_{2opt}^{*T} [k]_2 \right)^{*T} \\ &= [w]_{1\text{opt}}^{*T} [\Omega]_{12} [w]_{2\text{opt}}. \end{aligned} \tag{10}$$

Based on the three optimized coherences $\{\gamma_{\text{opt1}}, \gamma_{\text{opt2}}, \gamma_{\text{opt3}}\}$, two characteristic indicators of the coherence distribution in the different optimized channels, A_1 and A_2, are introduced in [28] and [29]

$$A_1 = \frac{|\gamma_{\text{opt1}}| - |\gamma_{\text{opt2}}|}{|\gamma_{\text{opt1}}|} \quad A_2 = \frac{|\gamma_{\text{opt1}}| - |\gamma_{\text{opt3}}|}{|\gamma_{\text{opt1}}|}. \tag{11}$$

III. Intensity-Driven AN Estimation

The AN concept in image processing has been introduced by Gordon and Rangayyan [30] in medical imagery. In each pixel (called *seed* when processed), a neighborhood of variable shape and dimensions is built by a region growing algorithm, containing only connected pixels that belong to the same statistical population as the seed. Only the values of pixels aggregated in the AN participate to the computation of the final value of the seed.

The main advantage of the method is to gather a significant number of samples in an estimation window where stationarity is preserved. ANs were also used for gray-level [31], [32] and color images [33], [34] filtering. In the context of SAR imaging, a multidimensional extension has also been proposed for adaptive-neighborhood filtering of multitemporal amplitude

data [35] and interferometric coherence and phase images [36], [37].

A. Intensity-Driven Region Growing

In the proposed method, only the intensity information is used to decide upon the pixel membership to the AN. Small homogenous regions within all six intensity images correspond to ground areas with an homogenous cover, which respect the stationarity hypothesis requirement for the estimation of the complex correlation in (3).

After initial complex multilooking a rough 6×6 noisy estimate of $[T]_6$ is available. All the available six intensity images simultaneously drive the region growing process. A 3×2 matrix is built containing only the elements of the main diagonal of $[T]_6$

$$[p](m,n) = \begin{bmatrix} [p]_1(m,n) \\ [p]_2(m,n) \\ [p]_3(m,n) \end{bmatrix} = \begin{bmatrix} [T_{11}]_{11}(m,n) & [T_{22}]_{11}(m,n) \\ [T_{11}]_{22}(m,n) & [T_{22}]_{22}(m,n) \\ [T_{11}]_{33}(m,n) & [T_{22}]_{33}(m,n) \end{bmatrix} \quad (12)$$

where $\{[p]_1, [p]_2, [p]_3\}$ are the bivariate vectors corresponding to the three lines of the real matrix $[p]$. Only the diagonal elements of the $[T]_{ii}$ matrices have been chosen as, after the Pauli basis transformation, they are related to the physical backscattering properties of the target. In the case of POLSAR data, each bivariate component of the $[p]$ matrix becomes scalars. Both the proposed algorithm and the corresponding equations remain unchanged [38].

The idea, based on Lee's sigma filter [39], is to retain in the AN only pixels which differ from the seed with less than twice the noise variation coefficient. According to the multilook SAR intensity image multiplicative noise model, the corresponding random variable is gamma distributed [21], [40]. For a distribution with parameters μ and σ, 95% of the samples lie in the interval $[\mu - 2\sigma/\mu, \mu + 2\sigma/\mu]$. The $\pm 2\sigma/\mu$ ($\mathrm{IDAN}_9 5$ thresholds from Fig. 1) interval ensures the population retained in the AN is statistically significant, and the following aggregation criterion is proposed for all the available bivariate vectors $[p]_i(k,l)$:

$$\frac{\|[p]_i(k,l) - [s](m,n)\|}{\|[s](m,n)\|} \leq 2\frac{\sigma_n}{\mu_n} \quad (13)$$

where $[s](m,n)$ is the seed vector. The variation coefficient σ_n/μ_n is a standard parameter in SAR imagery, which is constant in homogenous areas and equal to $1/\sqrt{L_{\mathrm{eq}}}$ (L_{eq} is the equivalent number of looks resulting from the initial averaging).

However, it is not desirable to use a single-step region growing algorithm with threshold $2\sigma_n/\mu_n$ (especially when the noise is strong, which is the case in the SAR imagery) under the risk that the region grows over boundaries, in contradiction with the goal of the region growing algorithm [Fig. 2(c)]. This is why a two-step region growing procedure is used [Fig. 2(d)]. In the first step, the aggregation threshold is set in order to retain only 50% of the statistical population [Fig. 2(b)]. With a single gamma distribution, the corresponding interval is $[\mu - (2/3)\sigma/\mu, \mu + (2/3)\sigma/\mu]$ (see IDAN_{50} thresholds in Fig. 1). The first aggregation criterion for each of the three bivariate vectors p_i, which yields the correct estimation of the seed, is

$$\frac{\|[p]_i(k,l) - [s](m,n)\|}{\|[s](m,n)\|} \leq \frac{2}{3}\frac{\sigma_n}{\mu_n}. \quad (14)$$

Using the $(2/3)\sigma_n/\mu_n$ threshold on the sum of the three channels, the resulting AN may possibly contain many holes, i.e., pixels that were not retained because they are affected by

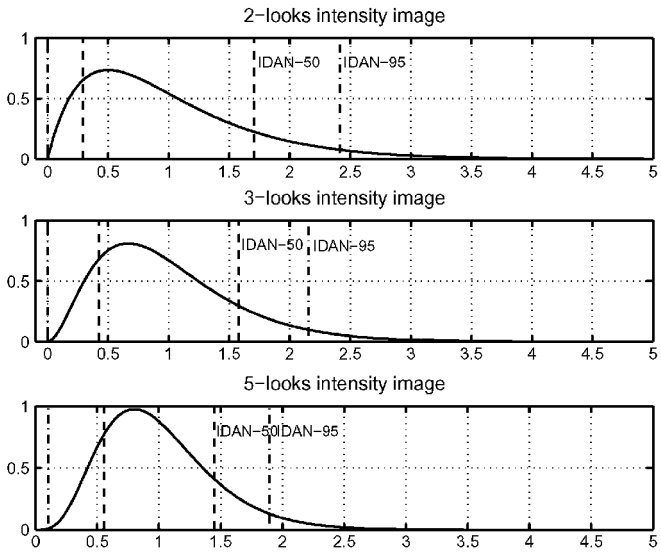

Fig. 1. Gamma pdf corresponding to multiplicative noise model for multilook SAR intensity images: $\mu = 1$ and $L = 2, 3, 5$. The aggregation thresholds IDAN_{50} (15) and IDAN_{95} (16) are set in order to retain only 50%, and 95% of the statistical population, respectively.

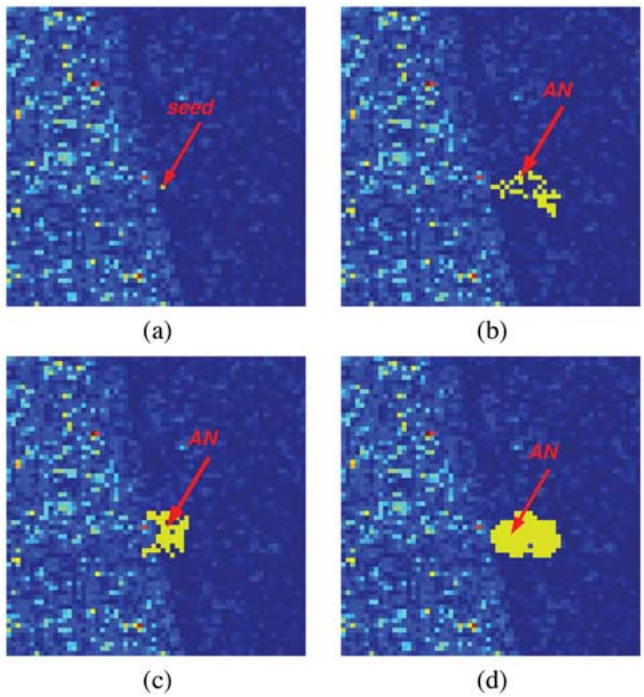

Fig. 2. Region growing process (64×64 pixels). (a) Two-look initial SAR intensity image. (b) One-step region growing with the IDAN_{50} threshold. (c) One-step region growing with the IDAN_{95} threshold. (d) Two-step region growing with the IDAN_{50} followed by the IDAN_{95} thresholds.

a "strong" instance of noise. However, these pixels belong to the same statistical population and should be retained in the AN. This is achieved in the second step (IDAN_{95} thresholds in Fig. 1), where *only pixels that were rejected in the first step* are reinspected with a less restrictive threshold $(2\sigma_n/\mu_n)$. The advantage of reinspecting only previously rejected pixels is that most of them are located *inside the convex hull of the AN determined in step one*, as they neighbor at least one of the pixels retained in the AN.

Based on this principle, the algorithm for constructing the AN consists of two steps.

Step I

1) *Rough estimation of the seed value*. Inside a 3×3 centered neighborhood, the median $\widehat{[p]}(m,n)$ is computed on each of the six component of the matrix, in order to yield a first estimate of the seed value. At this step, with a 3×3 neighborhood, the median is more appropriate than the mean (maximum likelihood estimator in homogenous areas), since the impulse response of the median filter is zero and a stepwise change in the input signal passes the median filter unaltered [41]. This property is very useful when data need to be smoothed, while blurring of the signal edges is not acceptable. At such an early stage of the region growing process, it is better to avoid any blurring effects around the edges in order to assure the signal stationarity in the next steps.
2) *Region growing*. All the eight direct neighbors $[p](k,l)$ of the seed are accepted inside the AN, provided they meet the following aggregation test, which merges the three distances corresponding to the three components of the multivariate vector $[p]_i$

$$\sum_{i=1}^{3} \frac{||[p]_i(k,l) - \widehat{[p]_i}(m,n)||}{||\widehat{[p]_i}(m,n)||} \leq 2\frac{\sigma_n}{\mu_n} \tag{15}$$

where μ_n and σ_n are the speckle mean and standard deviation. Then, the same procedure is applied for all of the neighbors of the newly included pixels and so on. The region growing iterates in this manner, until either the number of the pixels already included in the AN exceeds a predefined upper limit $N_{\max}$ or none of the neighbors verify the test condition given by (15). The pixels which have already been tested, but not accepted inside the AN (called *background pixels* in the sequel) are stored in a separate list.

Step II

1) *Refined estimation of the seed value*. A more reliable estimator $\overline{[p]}(m,n)$ of the selected seed value is obtained by averaging the pixels included in this "strict" AN obtained in Step I. The initial seed value $\widehat{[p]}(m,n)$ is now updated by $\overline{[p]}(m,n)$.
2) *Reinspection of the background pixels*. The background pixels $[p](o,p)$ of the list created in Step I are tested again and aggregated in the AN, provided that they meet the "enlarged" test condition

$$\sum_{i=1}^{3} \frac{||[p]_i(o,p) - \overline{[p]_i}(m,n)||}{||\overline{[p]_i}(m,n)||} \leq 6\frac{\sigma_n}{\mu_n}. \tag{16}$$

The test is less restrictive, as the inclusion threshold is larger than the one used in the first step of region growing.

It is important to notice that the intensity-driven region growing algorithm can be applied on one POLSAR acquisition, namely by employing only one polarimetric coherency matrix. The only difference is that the bivariate components $[p]_i$ $(i = 1, \ldots, 3)$ of the vector $[p](m,n)$ from (12) become scalars (diagonal elements of the available polarimetric coherency $[T]$)

$$[p](m,n) = \begin{bmatrix} [p]_1(m,n) \\ [p]_2(m,n) \\ [p]_3(m,n) \end{bmatrix} = \begin{bmatrix} [T]_{11}(m,n) \\ [T]_{22}(m,n) \\ [T]_{33}(m,n) \end{bmatrix}. \tag{17}$$

The same two-step region growing algorithm is then applied [38].

In summary, the proposed AN determination involves processing the vectorial image (as in the case of color images) mixed with multiplicative noise model (speckle noise is present in all SAR intensity images). Around each pixel, an AN is formed using a two-step region growing technique. It takes into account the information contained in all the intensity images of the available complex data. The use of ANs provides a larger set of samples for further processing, which respect the stationarity hypothesis.

B. Pol-InSAR Parameter Estimation

The conventional filtering method performs a complex averaging over a fixed size sliding window estimating the master and slave coherency matrices and the interferometric coherency matrix from (3). In this type of approach the number of pixels averaged may not be sufficient to reduce the estimation variance and the stationarity hypothesis is not always respected. The AN previously constructed solves these problems, considering that the phase stationarity over the neighborhood was ensured either by a standard flat earth fringe removal procedure or by a local phase slope estimation (in the case of unknown baseline or strong topography) [42], [43].

The proposed method allows to recompute the complex averaging over the largest possible neighborhood without loosing stationarity. In the case of the POL-InSAR data set, the matrices $[\Omega]_{12}$ and $[T]_{ii}, i = 1, \ldots, 2$ from (4) are estimated by replacing the ensemble average required by their definition, with a spatial average within the intensity-driven AN (IDAN)

$$\widehat{[T]_{ii}^{\mathrm{IDAN}}}(m,n) = \sum_{(k,l)\in AN(m,n)} [k]_i(k,l)[k]_i^{*T}(k,l) \tag{18}$$

$$\widehat{[\Omega]_{12}^{\mathrm{IDAN}}}(m,n) = \sum_{(k,l)\in AN(m,n)} [k]_1(k,l)[k]_2^{*T}(k,l). \tag{19}$$

In the case of single POLSAR data, using the multivariate vector from (17), the IDAN estimation technique of the polarimetric coherency matrix is implemented using (18).

A recent study presented in [44] determines speckle noise effects over the retrieved physical information in POLSAR data by means of the $H/\alpha/A$ decomposition. As the sample eigenvalues consist of asymptotically nonbiased estimators of the true eigenvalues, the minimum number of looks in order to neglect biases must be determined. The optimization algorithm of the

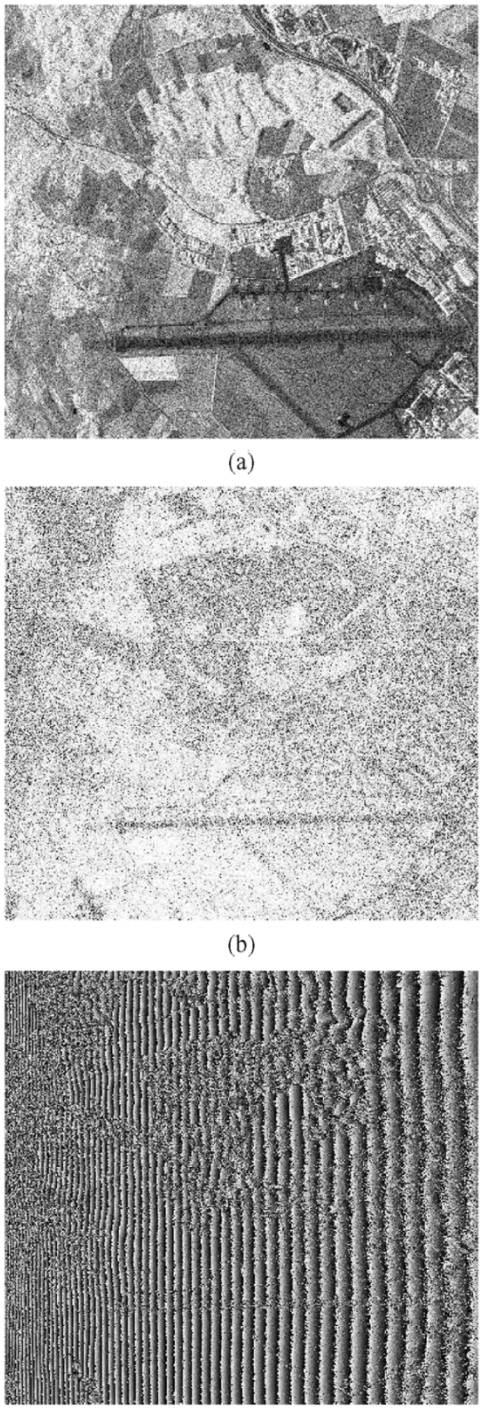

Fig. 3. POL-InSAR initial data (1540 × 1407 pixels). (a) Two-looks HH+VV master intensity (logarithmic scale). (b) Two-looks HH+VV initial coherence map. (c) Two-looks HH+VV initial interferogram.

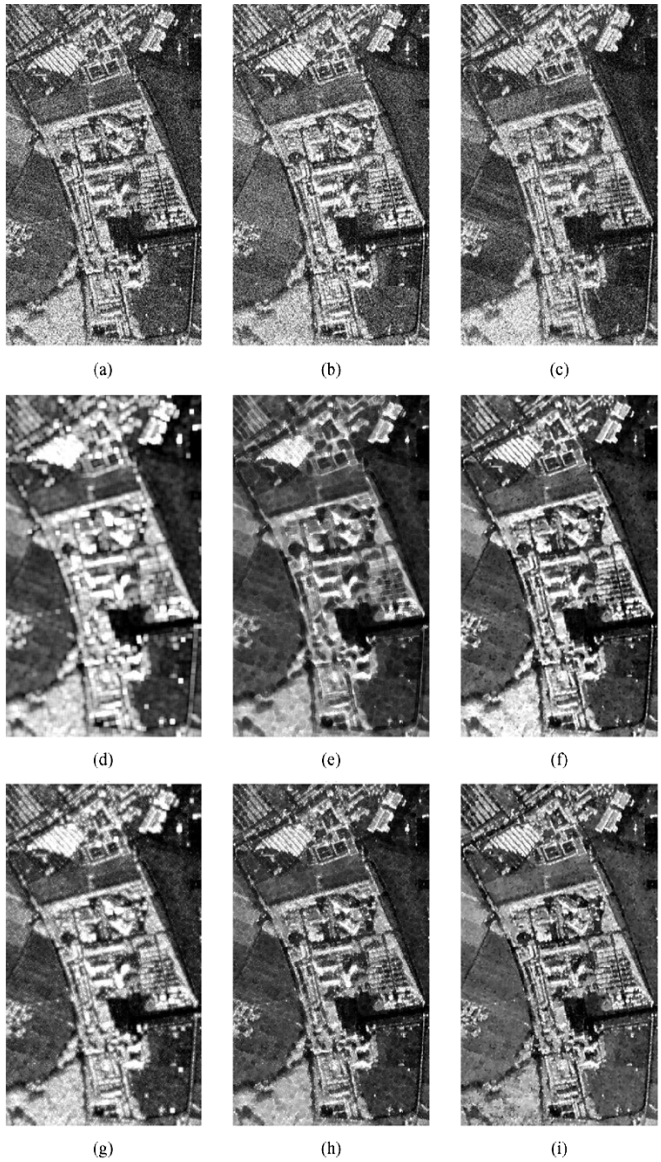

Fig. 4. Master intensity image filtering results (logarithmic scale) (526 × 310 pixels). (a)–(c) Original two-look intensity images (HH+VV, HH−VV and 2XX). (d)–(f) HH+VV boxcar, directional, and IDAN filters with complex multilooking. (g)–(i) HH+VV boxcar, directional, and IDAN filters with LLMMSE.

sample eigenvalues proposed in [44] does not succeed in correcting H with less than 81 looks and A values with less than 121 looks. The IDAN estimation provides such a high number of samples, while preserving stationarity and spatial resolution.

Depending on the desired POL-InSAR application, another refinement of the estimation method may be employed. For example in the case of forestry applications, the height of the trees is extracted from the interferometric coherency [45]. The strong multilooking induced by IDAN may affect the properties of the polarimetric scattering signatures of the targets (trees). In order to compensate these effects, a new technique which fuses the IDAN estimation and the LLMMSE from [20] is proposed (IDAN-LLMMSE). Instead of the directional windows, the previously constructed AN provides the necessary spatial support for the final LLMMSE estimation of the coherency matrix as

$$\widetilde{[T]}_6 = \widehat{[T]_6^{\mathrm{IDAN}}} + b\left([T]_6 - \widehat{[T]_6^{\mathrm{IDAN}}}\right). \tag{20}$$

$\widehat{[T]_6^{\mathrm{IDAN}}}$ represents the POL-InSAR coherency matrix computed in the obtained AN, while $b \in [0,1]$ is the filtering weight which is computed as in [20], except that, instead of using the average of the two span images from the interferometric couple, all the AN pixels of all the six available POLSAR span images are averaged.

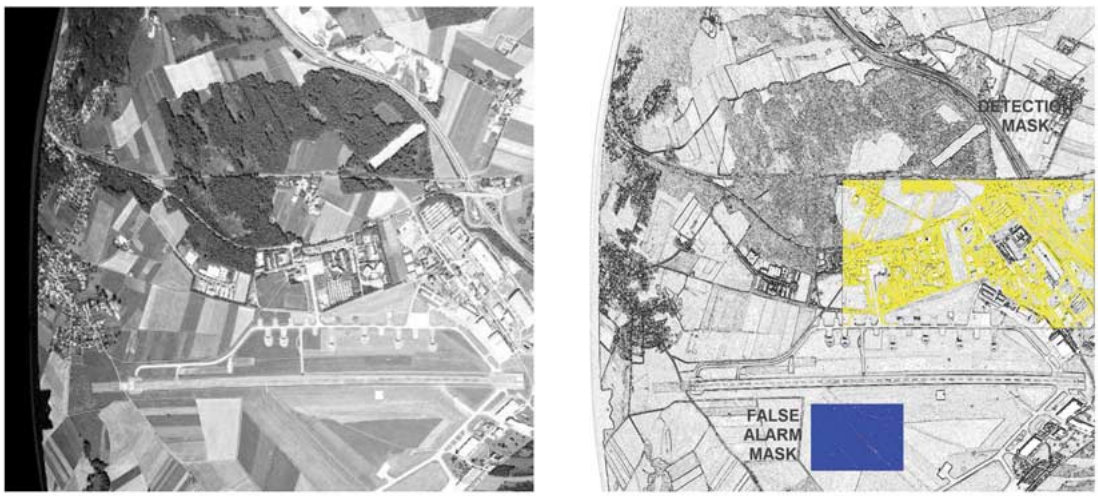

Fig. 5. Pol-InSAR data over the DLR headquarters (1540 × 1407 pixels). (a) Optical image resampled and registered on the available two-looks intensity images. (b) Sobel edge detection and thresholded reference areas used in the ROC analysis: blue for false alarm mask and yellow for detection mask.

IV. Results and Discussion

To illustrate the performances of the IDAN filtering method presented in Section III, results obtained with real airborne polarimetric interferometric SLC images are reported. The airborne data set was acquired in 1999 by an airborne experimental SAR system, E-SAR [46]. It represents a repeated pass, interferometric, fully polarimetric (monostatic mode) L-band (1.25 GHz) acquisition with a baseline of about 15 m. The spatial resolution is 1.5 m in range and azimuth. The target area is the Deutsches Zentrum für Luft-und Raumfahrt (DLR) headquarters (Oberpfaffenhofen area) from Wessling, Germany. It includes a large variety of zones, being one of the most used test POLSAR and POL-InSAR images [46], [47].

The SLC test images have 1540×2815 pixels each. After initial two-look complex multilooking, the initial estimate of the matrix $[T]_6$ is obtained (Fig. 3). On the master intensity image corresponding to the HH+VV polarization configuration the estimated equivalent number of looks is $L_{\text{est}} = 1.33$.

The results obtained by IDAN and IDAN-LLMMSE estimation algorithms are presented in Section IV-A–C. Several filters are also implemented for comparison purposes: boxcar filter and intensity driven directional neighborhood, with complex multilooking or with LLMMSE estimation. The implemented directional filter is similar to the one presented in [20], with the only difference that the window selection is driven on the sum of the six available span POL-InSAR images (all the diagonal terms of the $[T]_6$ matrix). The parameters used for POL-InSAR data IDAN filtering are: $N_{\max} = 50, (\sigma_n)/(\mu_n) = 0.87$. In order to assure the compatibility of the boxcar, directional filter and IDAN, in terms of filtering amount, the size of the chosen centered neighborhood of the boxcar was 7×7.

A. Speckle Reduction in POLSAR Span Images

In the case of nonadaptive filters, as the boxcar filter, the speckle reduction is always associated with strong edge-blurring effect [Fig. 4(d)]. The directional filter [Fig. 4(e)] is more satisfactory than the boxcar as the resulting edges are sharper. However, the fix size of the directional neighborhoods induces artifacts in the vicinity of thin details (smaller than the size of the neighborhoods). The boxcar LLMMSE [Fig. 4(g)] and directional LLMMSE [Fig. 4(h)] overcome these drawbacks, but the quality of achieved noise reduction is somewhat decreased. The IDAN filter [Fig. 4(f)] greatly reduces speckle over homogeneous areas, whereas structures are preserved. Thanks to the large number of homogeneous samples used in performing the multilooking, the achieved speckle reduction is more pronounced than other filters. A general remark for all the spatial filters is that the resulting filtered image has a "patchy" look, which is a known effect of purely spatial filtering. This effect is also observed for the IDAN. However, the IDAN-LLMMSE visually has less of this effect. The only drawback of the IDAN filter is in its high computational load.

In order to objectively assess the filtering performances, the receiver operating characteristics (ROC) are computed and further analyzed: first, a contour map is computed starting from the filtered HH+VV master POL-InSAR intensity image using conventional edge detectors. An optical image, previously resampled and registered on the initial master intensity image (Fig. 5), is used to obtain a contour map which provides the "ground truth" for the detection mask. A false alarm mask is also selected on the homogeneous fields around the runway.

Fig. 6 represents the three ROC curves for the edge detection on each of the filtered HH master intensity images. As it can be observed in Fig. 6(a), IDAN provides the best contour preservation. This can be explained by the fact that the IDAN detection is much higher for a given false alarm level. As expected, the directional filter (adaptive spatial filter) outperforms the boxcar (nonadaptive spatial filter). By introducing the LLMMSE method in the final filtering stage [Fig. 6(b)], directional LLMMSE and IDAN-LLMMSE provide much better performances than the boxcar LLMMSE with a higher detection probability.

B. Improved Estimation of the POL-InSAR Coherence Maps

The interferometric couple formed by the HH+VV component was chosen to illustrate the coherence filtering performances of

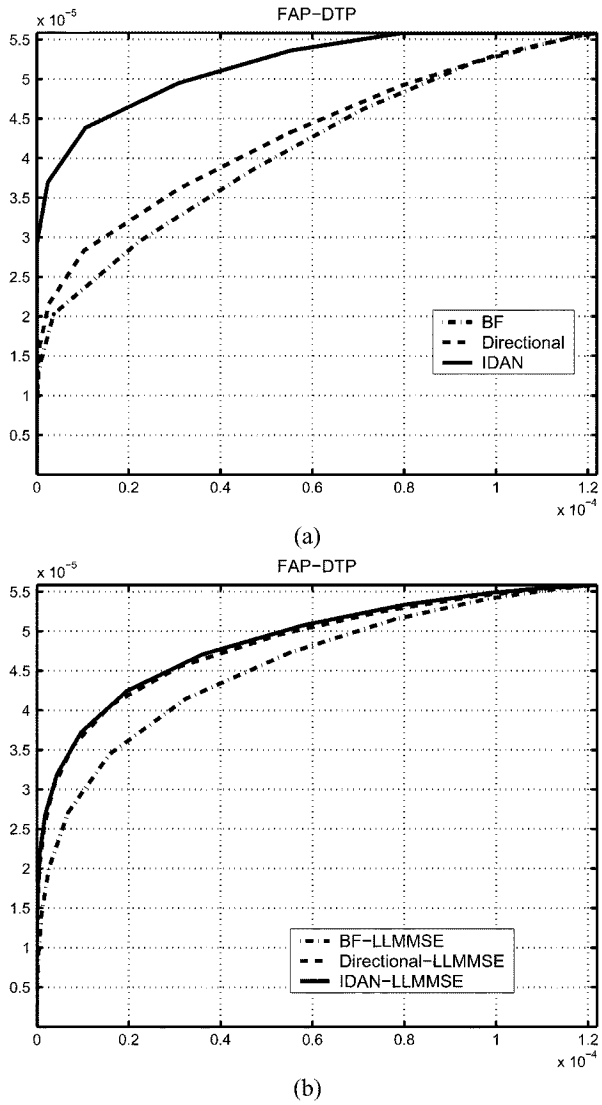

Fig. 6. Assessment of the edge detection performance in the Pol-InSAR filtered HH+VV master intensity images: receiver operating characteristics (detection probability versus false alarm probability). (a) Complex multilooking only. (b) LLMMSE estimation.

the six filters (see Fig. 7). One can observe that, also on this parameter, the IDAN [Fig. 7(c)] and IDAN-LLMMSE [Fig. 7(f)] outperform the other filters from a visual point of view: uniform areas are better smoothed, contours are better preserved and bias is more reduced. This can also be remarked in Tables I and II, which present the smoothing and bias reduction performances of the six filters computed over manually selected homogeneous regions of different coherence levels. An important decrease of the mean value after filtering is present over the low-coherence areas, i.e., where the bias was important, whereas in the high coherence region, the high level is preserved. Table II presents the standard deviation computed over all of the three regions. The minimum is obtained by IDAN, showing that this filter simultaneously performs the strongest bias and noise reductions inside homogeneous regions.

C. Pol-InSAR Parameter Extraction and Classification

The coherence optimization algorithm was also applied on the polarimetric interferometric coherency matrices filtered by

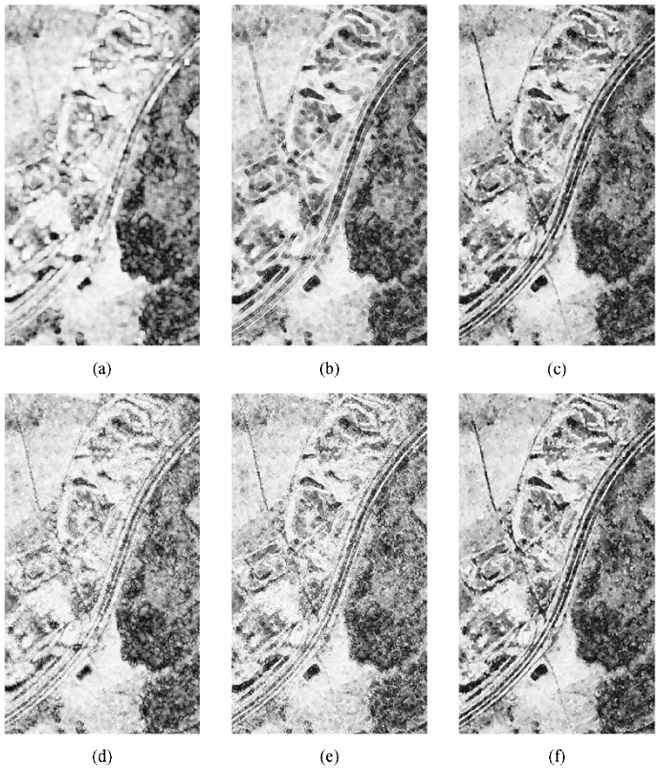

Fig. 7. HH+VV coherence map filtering results (526×310 pixels). (a)–(c) Boxcar, directional, and IDAN filters with complex multilooking. (d)–(f) Boxcar, directional, and IDAN filters with LLMMSE.

IDAN and IDAN-LLMMSE (Fig. 8). The additional information provided by the POL-InSAR parameters improves standard POLSAR classification results. As double bounce characterizes both building and vegetation, the A_1, A_2 decomposition reveals higher values over the stable building areas and lower values over the vegetation areas (high volume and temporal decorrelation) [29]. The IDAN-LLMSE filtered interferometric coherency provides the best results in terms of spatial resolution and discrimination between the two areas.

Physical parameters of the scatterers can directly be estimated from POLSAR data. In Fig. 9, $H-\alpha-A$ decomposition was performed on the master polarimetric coherency matrix filtered either by IDAN or IDAN-LLMMSE. Between the two filters, IDAN performs the best noise reduction, while IDAN-LLMMSE, ensures sharper edges, especially in the building areas. However, it is important to notice that this is the effect of the underestimation of the eigenvalues in the regions where the b parameter from (20) is close to one (no further multilooking is performed in the filtering stage). Hence, despite the high contrast, the estimated values of the POLSAR parameters are not reliable in the areas where the number of necessary samples is not reached.

Fig. 10 presents 2-D histograms of $H-\alpha$ parameters for the two proposed filters in three manually selected homogeneous areas. For comparison purposes, the mass center (MC) of the parameters estimated by a 15×30 boxcar complex multilooking is also plotted. An interesting effect can be observed, namely that as the value of entropy increases from Fig. 10(a)–(c), the bias reduction performed by IDAN becomes less important. This can be explained by the fact that high entropy values indicate strong

TABLE I
HH+VV COHERENCE MEAN OVER HOMOGENEOUS AREAS ON THE OBERPFAFFENHOFEN REGION

Region	Initial	Boxcar	Boxcar LLMMSE	Directional	Directional LLMMSE	IDAN	IDAN–LLMMSE
high	0.967	0.957	0.958	0.951	0.954	0.947	0.949
medium	0.854	0.703	0.707	0.663	0.688	0.638	0.648
low	0.794	0.301	0.366	0.305	0.376	0.257	0.278

TABLE II
HH+VV COHERENCE STANDARD DEVIATION OVER HOMOGENEOUS AREAS ON THE OBERPFAFFENHOFEN REGION

Region	Initial	Boxcar	Boxcar LLMMSE	Directional	Directional LLMMSE	IDAN	IDAN–LLMMSE
high	0.070	0.014	0.024	0.018	0.028	0.016	0.019
medium	0.178	0.105	0.134	0.115	0.147	0.081	0.096
low	0.201	0.157	0.194	0.160	0.208	0.086	0.117

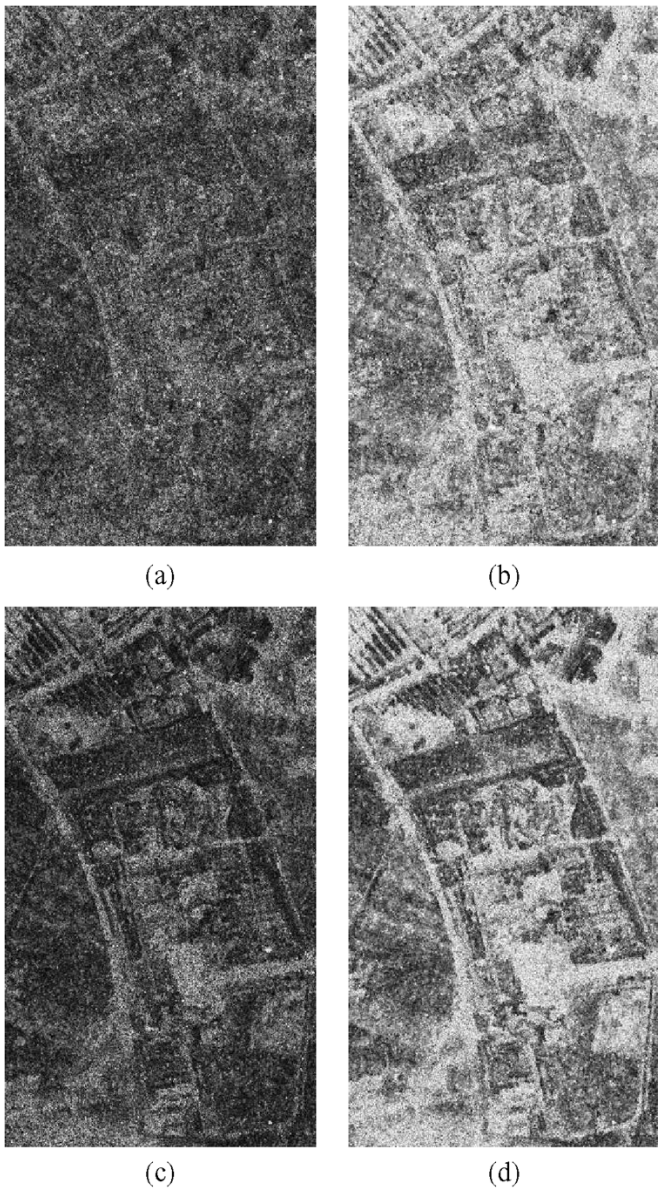

Fig. 8. A_1, A_2 decomposition of the interferometric coherency matrix (526×310 pixels). (a) A_1 and (b) A_2, parameters estimated from the IDAN filtered interferometric coherency matrix. (c) A_1 and (d) A_2, parameters estimated from the IDAN-LLMMSE filtered interferometric coherency matrix.

variation of the target scattering mechanisms inside the three-dimensional (3-D) (2-D spatial+1-D polarimetric) estimation

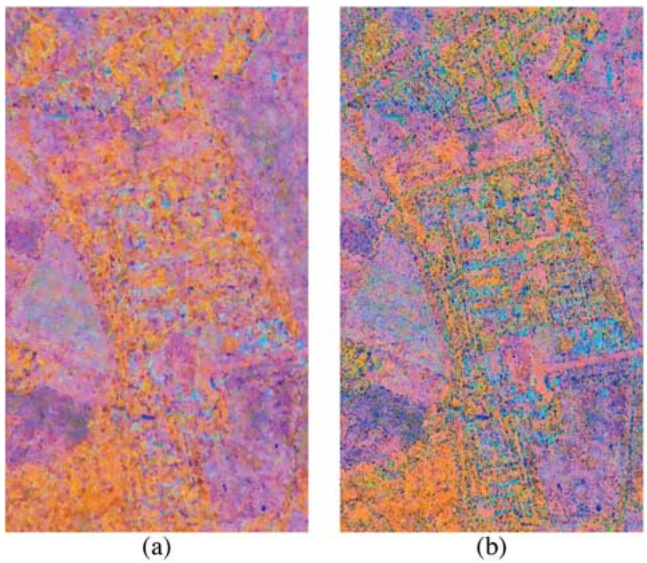

Fig. 9. $H - \alpha - A$ color RGB composition on the master polarimetric coherency matrix (526×310 pixels). (a) IDAN filtering. (b) IDAN-LLMMSE filtering.

window. In such areas, the AN has rather small dimensions, thus it cannot provide enough complex multilooking for an unbiased estimation of the α parameter. Despite the fact that the IDAN complex multilooking behaves much better than IDAN-LLMMSE in terms of reducing the noise variance, the latter [Fig. 10(d)–(f)] provides reliable bias reduction in all cases, even with high entropy values. Hence, in the classification applications where high entropy targets are investigated, the IDAN-LLMMSE parameter estimation technique provides better results than IDAN complex multilooking.

The behavior of the two filters can be observed in Fig. 11, which presents the results of the Wishart classification using as input images the master coherency filtered by either IDAN or IDAN-LLMMSE. As expected, due to the strongest noise and bias reduction on the homogenous area (fields, runway), the obtained results are much more regularized for the IDAN filtered coherency. The thin structures (buildings) are very well defined in both cases. Comparing the IDAN and IDAN-LLMMSE classification map with the optical image, the IDAN classification reveals much more spatial information than the IDAN-LLMSE classification. It is difficult to separate runway class from surrounding fields classes in Fig. 11(b), while with IDAN

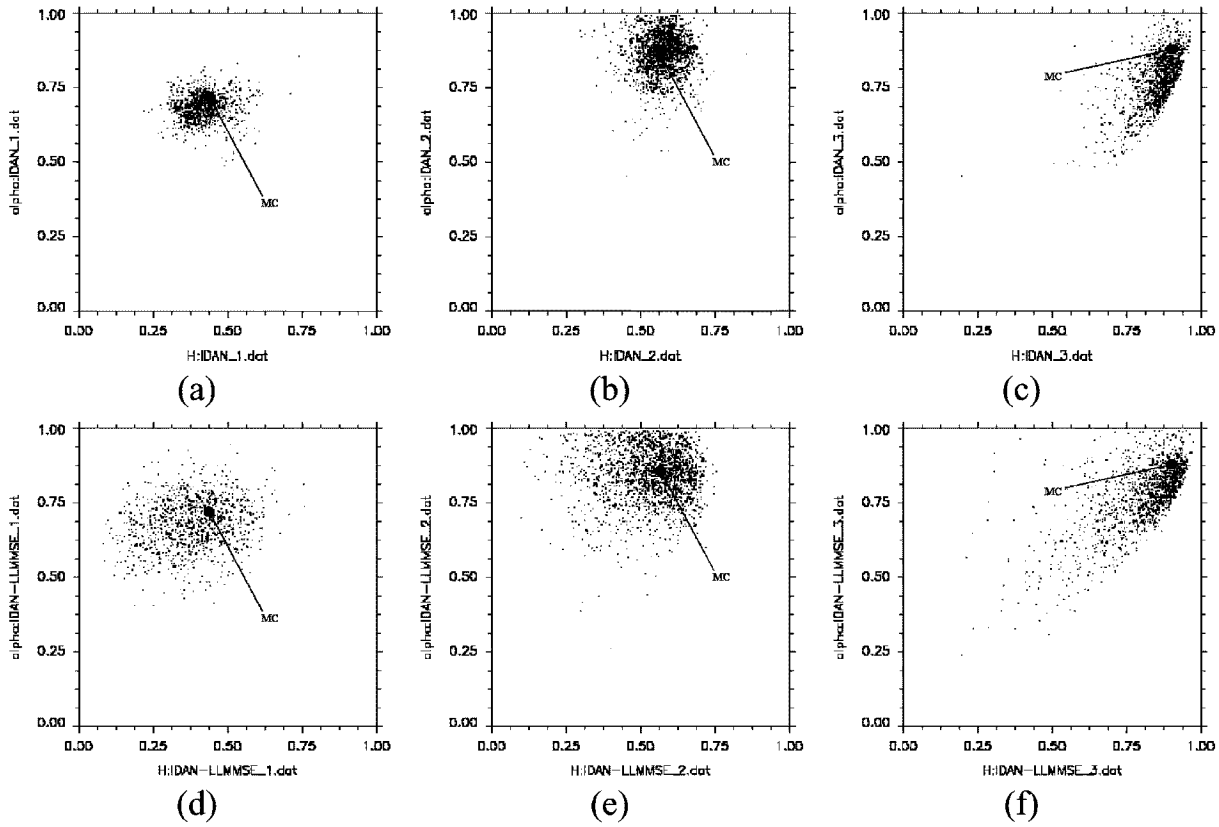

Fig. 10. $H - \alpha$ distribution on various homogeneous areas. (a)–(c) IDAN with complex multilooking. (d)–(f) IDAN with LLMMSE. MC is the boxcar MC of the selected region, estimated with a 15(range) × 30(azimuth) complex multilooking.

[Fig. 11(a)] the runway classification is better defined. Two forest areas clearly appear in the upper left region of Fig. 11(a). These classes are mixed in the IDAN-LLMMSE classification.

In summary, the overall performance of IDAN and IDAN-LLMMSE, POLSAR, and POL-InSAR filtering techniques has been evaluated at different stages. First, the ROC analysis and the bias reduction tables have been applied on low-level attributes (POL-InSAR intensities and coherence maps). Medium level physical parameters of the scatterers were computed and the influence of the proposed filtering method have been investigated (H, α, A, A_1, and A_2). A final high-level Wishart classification have been employed and the obtained results were discussed in correlation with the visual information of the available optical image.

As mentioned earlier, the critical point of this filtering procedure concerns the determination of the homogeneous area surrounding a pixel. One of the main advantages of the proposed IDAN technique relies on the fact that homogeneity is estimated using the three POLSAR or six POL-InSAR intensities, which are directly available with a very small number of looks. More complex statistical measures, based on the polarimetric or interferometric information [48] could be used, but they would require a much higher number of initial looks. In the POLSAR case, the criterion that merges the coherency matrix diagonal elements (17) allows to take an important part of the polarimetric information into account [49]. However, for POL-InSAR data sets, intensity variations may be, in some cases, unrelated to the coherence information. Over distributed media, like forest, it has been recently shown [29] that the average span image may be an unsuitable parameter, involving that the resulting estimated seeds may not contain pixels with homogeneous coherence. These areas correspond to high entropy values and, as observed in Fig. 10(c), the bias reduction is less important. In such cases, the IDAN-LLMMSE filter, by performing the local stationarity test twice within all the intensity images corresponding to the available polarization configurations, gives better results since less filtering is performed and the local backscattering mechanisms are better preserved.

V. Conclusion

A new method of filtering coherency matrices of polarimetric or interferometric data has been presented. The proposed filter uses ANs as spatial support, derived with respect to the intensity information. All the available intensity images of the POL-InSAR data are combined in the region growing procedure, to ensure the stationarity assumption. The proposed filter recomputes the polarimetric and interferometric coherency matrices, either by direct complex multilooking or from the LLMMSE estimator of the coherency matrix.

The experimental results have proved that the noise is greatly reduced, while the contours and fine details are preserved and the blurring effect is avoided. The reliability of the obtained results is demonstrated by either subjective assessment or by conventional objective analysis (ROC characteristics and bias reduction tables). Physical parameters of the scatterers were computed and the influence of the proposed filtering method

Fig. 11. Wishart $H-\alpha$ classification of master coherency matrix (500×500 pixels). (a) Classification result using IDAN filtered $[T]_{11}$. (b) Classification result using IDAN-LLMMSE filtered $[T]_{11}$. (c) Coregistered optical image showing different land covers, related to the obtained classes, for comparison purposes.

has been investigated for POLSAR (H, α, A) and POL-InSAR (A_1, A_2) parameters. A final Wishart classification has been employed and the obtained results were discussed and compared to the available optical image. All these features make the presented adaptive filtering algorithms an effective and powerful tool for noise or bias reduction for polarimetric or interferometric data processing.

The general conclusion is that the choice of the filtering algorithm to be used on a given POLSAR or POL-InSAR data set still remains application specific. The IDAN filter is a good compromise between variance or bias reduction and preservation of the spatial resolution, which makes it very useful for automatic unsupervised activities (edge detection, segmentation or automatic classification). However, in the case of supervised activity as direct visual interpretation or scattering signature assessment of pointwise targets, the IDAN-LLMMSE filter is more efficient.

ACKNOWLEDGMENT

The authors would like to thank the German Aerospace Center (DLR), Wessling, Germany, for providing the high-resolution polarimetric interferometric E-SAR images and the anonymous reviewers for helpful comments and suggestions.

REFERENCES

[1] R. Touzi, A. Lopes, J. Bruniquel, and P. W. Vachon, "Coherence estimation for SAR imagery," *IEEE Trans. Geosci. Remote Sens.*, vol. 37, no. 1, pp. 135–149, Jan. 1999.

[2] J. S. Lee, K. W. Hoppel, S. A. Mango, and A. R. Miller, "Intensity and phase statistics of multilook polarimetric and interferometric SAR imagery," *IEEE Trans. Geosci. Remote Sens.*, vol. 32, no. 5, pp. 1017–1028, Sep. 1994.

[3] S. R. Cloude, "Group theory and polarization algebra," *OPTIK*, vol. 75, pp. 26–36, 1986.

[4] S. R. Cloude and E. Pottier, "A review of target decomposition theorems in radar polarimetry," *IEEE Trans. Geosci. Remote Sens.*, vol. 34, no. 2, pp. 498–518, Mar. 1996.

[5] S. R. Cloude and E. Pottier, "An entropy based classification scheme for land applications of polarimetric SAR," *IEEE Trans. Geosci. Remote Sens.*, vol. 35, no. 1, pp. 68–78, Jan. 1997.

[6] J. S. Lee, M. R. Grunes, T. L. Ainsworth, D. Li-Jen, D. L. Schuler, and S. R. Cloude, "Unsupervised classification using polarimetric decomposition and the complex Wishart classifier," *IEEE Trans. Geosci. Remote Sens.*, vol. 37, no. 5, pp. 2249–2258, Sep. 1999.

[7] L. Ferro-Famil, E. Pottier, and J. S. Lee, "Unsupervised classification of multifrequency and fully polarimetric SAR images based on the H/A/Alpha-Wishart classifier," *IEEE Trans. Geosci. Remote Sens.*, vol. 39, no. 11, pp. 2332–2342, Nov. 2001.

[8] S. R. Cloude and K. P. Papathanassiou, "Polarimetric SAR interferometry," *IEEE Trans. Geosci. Remote Sens.*, vol. 36, no. 5, pp. 1551–1565, Sep. 1998.

[9] K. P. Papathanassiou, A. Reigber, R. Scheiber, R. Horn, A. Moreira, and S. R. Cloude, "Airborne polarimetric SAR interferometry," in *Proc. Geosci. Remote Sens. Symp.*, vol. IV, Seattle, WA, 1998, pp. 1901–1903.

[10] J. S. Lee, I. Jurkevich, P. Dewaele, P. Wambacq, and A. Oosterlinck, "speckle filtering of synthetic aperture radar images: A review," *Remote Sens. Rev.*, vol. 8, pp. 313–340, 1994.

[11] R. Touzi, "A review of speckle filtering in the context of estimation theory," *IEEE Trans. Geosci. Remote Sens.*, vol. 40, no. 11, pp. 2392–2404, Nov. 2002.

[12] J.-S. Lee, "Refined filtering of image noise using local statistics," *Comput. Graph. Image Process.*, vol. 15, pp. 380–389, 1981.

[13] D. T. Kuan, A. A. Sawchuk, T. C. Strand, and P. Chavel, "Adaptive noise smoothing filter for images with signal dependent noise," *IEEE Trans. Pattern Anal. Mach. Intell.*, vol. 7, no. 2, pp. 165–177, Mar. 1985.

[14] A. Lopés, E. Nezry, R. Touzi, and H. Laur, "Structure detection, and statistical adaptive filtering in SAR images," *Int. J. Remote Sens.*, vol. 14, no. 9, pp. 1735–1758, 1993.

[15] M. Datcu, K. Seidel, and M. Walessa, "Spatial information retrieval from remote-sensing images—Part 1: Information theoretical perspective," *IEEE Trans. Geosci. Remote Sens.*, vol. 36, no. 5, pp. 1431–1445, Sep. 1998.
[16] M. Schroder, K. Seidel, and M. Datcu, "Spatial information retrieval from remote-sensing images, Part 2: Gibbs-markov random fields," *IEEE Trans. Geosci. Remote Sens.*, vol. 36, no. 5, pp. 1446–1455, Sep. 1998.
[17] Y. Wu and H. Maître, "Smoothing speckled synthetic aperture radar images by using maximum homogeneous region filters," *Opt. Eng.*, vol. 31, no. 8, pp. 1785–1792, Aug. 1992.
[18] J. M. Nicolas, F. Tupin, and H. Maître, "Smoothing speckled SAR images by using maximum homogeneous region filters: An improved approach," in *Proc. IEEE Int. Geosci. Remote Sens. Symp.*, vol. III, Sydney, NSW, Australia, Jul. 2001, pp. 1503–1505.
[19] W. Hagg and M. Sties, "Efficient speckle filtering of SAR images," in *Proc. IEEE Int. Geosci. Remote Sens. Symp.*, Pasadena, CA, 1994, pp. 2140–2142.
[20] J. S. Lee, S. R. Cloude, K. Papathanassiou, M. R. Grunes, and I. H. Woodhouse, "Speckle filtering and coherence estimation of polarimetric SAR interferometry data for forest applications," *IEEE Trans. Geosci. Remote Sens.*, vol. 41, no. 10, pp. 2254–2263, Oct. 2003.
[21] J. W. Goodman, "Statistical analysis based on certain multivariate complex Gaussian distribution (An introduction)," *Ann. Math. Statist.*, pp. 152–176, 1963.
[22] J. R. Huynen, "Measurement of the target scattering matrix," *Proc. IEEE*, vol. 53, no. 8, pp. 936–946, Aug. 1965.
[23] E. Krogager, "New decomposition of the radar target scattering matrix," *Electron. Lett.*, vol. 26, no. 18, pp. 1525–1527, 1990.
[24] W. L. Cameron and L. K. Leung, "Feature motivated polarization scattering matrix decomposition," in *Proc. IEEE Int. Radar Conf.*, Arlington, VA, USA, 1990, pp. 549–557.
[25] A. Freeman and S. L. Durden, "A three-component scattering model for polarimetric SAR data," *IEEE Trans. Geosci. Remote Sens.*, vol. 36, no. 3, pp. 963–973, May 1998.
[26] R. Touzi, "Target scattering decomposition of one-look and multilook SAR data using a new coherent scattering model: The TSVM," in *Proc. IEEE Int. Geosci. Remote Sens. Symp.*, vol. IV, 2004, pp. 2491–2494.
[27] A. Reigber, M. Neumann, S. Guillaso, M. Jager, and O. Hellwich, "PolInSAR data processing with RAT (radar tools)," in *POLinSAR 2005 Workshop*, Franscati, Italy, 2005, CD-ROM, Paper no. 24.
[28] L. Ferro-Famil, E. Pottier, and J. S. Lee, *Unsupervised Classification of Natural Scene from Polarimetric Inteferometric SAR Data*, ed, C. H. Chen, Ed, Singapore: World Scientific, 2003.
[29] J. S. Lee, M. R. Grunes, T. Ainsworth, I. Hajnsek, T. Mette, and K. P. Papathanassiou, "Forest classification based on L-band polarimetric and inteferometric SAR data," in *POLinSAR 2005 Workshop*, Franscati, Italy, 2005, CD-ROM, Paper no. 43.
[30] R. Gordon and R. M. Rangayyan, "Feature enhancement of film mammograms using fixed and adaptive neighborhoods," *Appl. Opt.*, vol. 23, no. 4, pp. 560–564, Feb. 1984.
[31] R. B. Paranjape, T. F. Rabie, and R. M. Rangayyan, "Image restoration by adaptive-neighborhood noise substraction," *Appl. Opt.*, vol. 33, no. 14, pp. 1861–1869, 1994.
[32] R. M. Rangayyan, M. Ciuc, and F. Faghih, "Adaptive-neighborhood filtering of images corrupted by signal-dependent noise," *Appl. Opt.*, vol. 37, no. 20, pp. 4477–4487, May 1998.
[33] M. Ciuc, R. M. Rangayyan, T. Zaharia, and V. Buzuloiu, "Adaptive neighborhood filters for color image filtering," in *Proc. SPIE Nonlinear Image Process.*, vol. 3304, 1998, pp. 277–286.
[34] M. Ciuc, R. M. Rangayyan, T. Zaharia, and V. Buzuloiu, "Filtering noise in color images using adaptive-neighborhood statistics," *J. Electron. Imaging*, vol. 9, pp. 484–494, 2000.
[35] M. Ciuc, Ph. Bolon, E. Trouvé, V. Buzuloiu, and J. P. Rudant, "Adaptive-neighborhood speckle removal in multitemporal synthetic aperture radar images," *Appl. Opt.*, vol. 40, no. 6, pp. 5954–5966, 2001.
[36] G. Vasile, E. Trouvé, M. Ciuc, and V. Buzuloiu, "General adaptive neighborhood technique for improving SAR interferometric coherence and phase estimation," *J. Opt. Soc. Amer. A*, vol. 21, no. 8, pp. 1455–1464, Aug. 2004.
[37] G. Vasile, E. Trouvé, M. Ciuc, P. Bolon, and V. Buzuloiu, "Improving coherence estimation for high resolution polarimetric SAR interferometry," in *Proc. Geosci. Remote Sens. Symp.*, vol. III, Anchorage, AK, 2004, pp. 1796–1799.
[38] ——, "Intensity-driven-adaptive-neighborhood technique for POLSAR parameters estimation," in *Proc. Geosci. Remote Sens. Symp.*, vol. VIII, Seoul, Korea, 2005, pp. 5509–5512.
[39] J. S. Lee, "Digital noise smoothing and the sigma filter," *Comput. Vis., Graph. Image Process.*, vol. 21, pp. 255–269, 1983.
[40] J. W. Goodman, "Some fundamental properties of speckle," *J. Opt. Soc. Amer. A*, vol. 66, pp. 1145–1149, 1976.
[41] J. Astola, P. Haavisto, and Y. Neuvo, "Vector median filters," *Proc. IEEE*, vol. 78, no. 4, pp. 678–688, Apr. 1990.
[42] E. Trouvé, J. M. Nicolas, and H. Maitre, "Improving phase unwrapping techniques by the use of local frequency estimates," *IEEE Trans. Geosci. Remote Sens.*, vol. 36, no. 6, pp. 1963–1972, Dec. 1998.
[43] E. Trouvé, M. Caramma, and H. Maître, "Fringe detection in noisy complex interferograms," *Appl. Opt.*, vol. 35, no. 20, pp. 3799–3806, Jul. 1996.
[44] C. Lopez-Martinez, E. Pottier, and S. R. Cloude, "Statistical assessment of eigenvector-based target decomposition theorems in radar polarimetry," *IEEE Trans. Geosci. Remote Sens.*, vol. 43, no. 9, pp. 2058–2074, Sep. 2005.
[45] S. R. Cloude, K. P. Papathanassiou, and W. M. Boerner, "A fast method for vegetation correction in topographic mapping using polarimetric radar interferometry," in *Proc. EUSAR 2000*, Munich, Germany, May 2000, pp. 261–264.
[46] S. R. Cloude, K. P. Papathanassiou, A. Reigber, and W. M. Boerner, "Multi-frequency polarimetric SAR interferometry for vegetation structure extraction," in *Proc. Geosci. Remote Sens. Symp.*, vol. I, Honolulu, HI, 2000, pp. 129–131.
[47] D. Borghys, C. Perneel, and M. Acheroy, "Edge and line detection in polarimetric SAR images," in *Proc. Int. Conf. Pattern Recognit., Int. Assoc. Pattern Recognit.*, vol. II, Quebec, ON, Canada, 2002, pp. 921–924.
[48] J. Schou and H. Skriver, "Restoration of polarimetric SAR images using simulated annealing," *IEEE Trans. Geosci. Remote Sens.*, vol. 39, no. 9, pp. 2005–2016, Sep. 2001.
[49] J. S. Lee, D. L. Schuler, and T. L. Ainsworth, "Scattering model based speckle filtering of polarimetric SAR data," in *Proc. 5th Eur. Conf. SAR*, vol. V, Ulm, Germany, 2004, pp. 203–207.

Gabriel Vasile (S'06) received the Engineer degree in electrical engineering and computer science and the M.S. degree in image, shapes, and artificial intelligence from the University Politehnica of Bucharest, Bucharest, Romania, in 2003 and 2004. Since 2004, he has been working on his Ph.D. dissertation on SAR multivariate signal processing with joint supervision from both Politehnica of Bucharest and University of Savoie, Annecy, France, in the framework of the French multilaboratory MEGATOR project.

His research interests are signal and image processing, polarimetric and interferometric SAR applications, and glacier monitoring.

Emmanuel Trouvé (M'00) received the Engineer degree in electrical engineering from the Ecole Nationale Supérieure de Techniques Avancées, Paris, France, in 1990, and the Ph.D. degree in signal and image processing from Ecole Nationale Supérieure des Télécommunications, Paris, France, in 1996.

From 1996 to 1998, he worked with Thomson Marconi Sonar in Underwater Acoustic and Signal Processing. Since September 1998, he has been an Associate Professor of signal processing and computer vision at Ecole Supérieure d'Ingénieurs d'Annecy, University of Savoie, Annecy, France, and works in the Computer Science, System, Information and Knowledge Processing Laboratory (LISTIC). His research interests are SAR image processing and data fusion in remote sensing. He coordinates the French multilaboratory MEGATOR project (Monitoring the Evolution of Alpine Glaciers by Optical and Radar Remote Sensing).

Dr. Trouvé is a member of the IEEE Geoscience and Remote Sensing Society Data Fusion Technical Committee.

Jong-Sen Lee (M'69–SM'91–F'97–LF'05) received the B.S. degree from the National Cheng-Kung University, Tainan, Taiwan, R.O.C., in 1963, and the M.A. and Ph.D. degrees from Harvard University, Cambridge, MA, in 1965 and 1969, respectively.

He is currently Head of the Image Science Section, Remote Sensing Division, Naval Research Laboratory, Washington, DC, where he is the Principal Investigator for several remote sensing programs on polarimetric SAR and interferometric SAR. He has developed several speckle filtering algorithms that have been implemented in many GIS, such as ERDAS, PCI, and ENVI, etc. His research covers a wide spectrum of areas, from control theory, operation research, and radiative transfer to SAR and polarimetric SAR image processing. He has investigated SAR image segmentation, inverse SAR, polarimetric SAR imagery statistics and speckle filtering, SAR polarimetry, and terrain/land-use classification and applications. His current research interests are in the area of SAR polarimetry, scattering signature modeling, polarimetric SAR calibration, polarimetric SAR interferometry, and unsupervised segmentation and classification using polarimetric and interferometric SAR data. He was granted a U.S. patent for the invention of a topography measurement technique using polarimetric SAR. He has published more than 60 papers in refereed journals and more than 150 papers in conference proceedings and has given tutorials at IGARSS'97 and IGARSS'98.

Dr. Lee was presented the Best Paper Award and the Best Poster Award at the Third and Fourth European Conference on Synthetic Aperture Radar (EUSAR2000 and EUSAR2002), respectively. He was made a Fellow of IEEE for his contribution toward information processing of SAR and polarimetric SAR imagery. He has chaired and organized many sessions in international conferences and is currently an Associate Editor of the IEEE TRANSACTIONS ON GEOSCIENCE AND REMOTE SENSING.

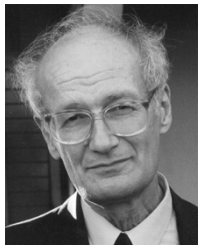

Vasile Buzuloiu (M'91–SM'05) received the M.S. and Ph.D. degrees in electronics from the University Politehnica Bucharest, Bucharest, Romania, in 1959 and 1980, respectively, and the M.S. degree in mathematics from "Universitatea Bucuresti" Bucharest, Romania, in 1971.

He is a professor with the Department of Applied Electronics and Information Engineering, University Politehnica Bucharest. He also heads the Image Processing and Analysis Laboratory and is a Research Associate with CERN, Geneva, Switzerland. His scientific interests cover mathematical modeling, statistical decisions, encryption, digital signal processing, image processing and analysis systems, and image processing applications. He also holds the title of Honorary Professor of the University Transilvania, Brasov, Romania (2001). Since 1994, he has held various positions of Invited Professor at French Universities (INSA de Lyon, ESIA-Université de Savoie, Université St. Etienne, Université Poitiers, INP Toulouse, etc.). Since 1995, he has been the Director of the Spring International School "Multidimensional Signal Processing and Analysis: Methods, Algorithms, Technologies, Applications" which is organized yearly at the University Politehnica Bucharest.

Dr. Buzuloiu received the "Traian Vuia" Award of the Romanian Academy (1985) for the first digital image analysis system developed in Romania. He is a Member of SPIE, Color Group (Great Britain), and the Romanian Society for Applied Mathematics.